SLAC-PUB-9869

First Measurement of the B -> pi lepton neutrino And B -> rho(omega) lepton neutrino Branching Fractions

Submitted to Physical Review Letters

Stanford Linear Accelerator Center, Stanford University, Stanford, CA 94309

Work supported by Department of Energy contract DE–AC03–76SF00515.

CLNS 96-1419
CLEO 96-9

First Measurement of the $B \to \pi\ell\nu$ and $B \to \rho(\omega)\ell\nu$ Branching Fractions

CLEO Collaboration

(July 1, 1996)

Abstract

CLEO has studied B decays to the final states $\pi\ell\nu$, $\rho\ell\nu$, and $\omega\ell\nu$, where $\ell = e$ or μ. We fully reconstruct these modes using a measurement of the missing energy and momentum in each event to infer the neutrino momentum. With the B^0 and B^+ modes combined according to isospin predictions for the relative partial widths, we obtain $\mathcal{B}(B^0 \to \pi^-\ell^+\nu) = (1.8 \pm 0.4 \pm 0.3 \pm 0.2) \times 10^{-4}$ and $\mathcal{B}(B^0 \to \rho^-\ell^+\nu) = (2.5 \pm 0.4^{+0.5}_{-0.7} \pm 0.5) \times 10^{-4}$, where the errors are statistical, systematic and the estimated model-dependence. We also estimate $|V_{ub}| = (3.3 \pm 0.2^{+0.3}_{-0.4} \pm 0.7) \times 10^{-3}$.

13.20.He,14.40.Nd,12.15.Hh

J.P. Alexander,[1] C. Bebek,[1] B.E. Berger,[1] K. Berkelman,[1] K. Bloom,[1] D.G. Cassel,[1] H.A. Cho,[1] D.M. Coffman,[1] D.S. Crowcroft,[1] M. Dickson,[1] P.S. Drell,[1] D.J. Dumas,[1] R. Ehrlich,[1] R. Elia,[1] P. Gaidarev,[1] B. Gittelman,[1] S.W. Gray,[1] D.L. Hartill,[1] B.K. Heltsley,[1] C.D. Jones,[1] S.L. Jones,[1] J. Kandaswamy,[1] N. Katayama,[1] P.C. Kim,[1] D.L. Kreinick,[1] T. Lee,[1] Y. Liu,[1] G.S. Ludwig,[1] J. Masui,[1] J. Mevissen,[1] N.B. Mistry,[1] C.R. Ng,[1] E. Nordberg,[1] J.R. Patterson,[1] D. Peterson,[1] D. Riley,[1] A. Soffer,[1] C. Ward,[1] P. Avery,[2] C. Prescott,[2] S. Yang,[2] J. Yelton,[2] G. Brandenburg,[3] R.A. Briere,[3] T. Liu,[3] M. Saulnier,[3] R. Wilson,[3] H. Yamamoto,[3] T. E. Browder,[4] F. Li,[4] J. L. Rodriguez,[4] T. Bergfeld,[5] B.I. Eisenstein,[5] J. Ernst,[5] G.E. Gladding,[5] G.D. Gollin,[5] I. Karliner,[5] M. Palmer,[5] M. Selen,[5] J.J. Thaler,[5] K.W. Edwards,[6] M. Ogg,[6] A. Bellerive,[7] D.I. Britton,[7] R. Janicek,[7] D.B. MacFarlane,[7] K.W. McLean,[7] P.M. Patel,[7] A.J. Sadoff,[8] R. Ammar,[9] P. Baringer,[9] A. Bean,[9] D. Besson,[9] D. Coppage,[9] N. Copty,[9] R. Davis,[9] N. Hancock,[9] S. Kotov,[9] I. Kravchenko,[9] N. Kwak,[9] S.Anderson,[10] Y. Kubota,[10] M. Lattery,[10] J.J. O'Neill,[10] S. Patton,[10] R. Poling,[10] T. Riehle,[10] A. Smith,[10] V. Savinov,[10] M.S. Alam,[11] S.B. Athar,[11] I.J. Kim,[11] Z. Ling,[11] A.H. Mahmood,[11] H. Severini,[11] S. Timm,[11] F. Wappler,[11] J.E. Duboscq,[12] R. Fulton,[12] D. Fujino,[12] K.K. Gan,[12] K. Honscheid,[12] H. Kagan,[12] R. Kass,[12] J. Lee,[12] M. Sung,[12] A. Undrus,[12*] C. White,[12] R. Wanke,[12] A. Wolf,[12] M.M. Zoeller,[12] B. Nemati,[13] S.J. Richichi,[13] W.R. Ross,[13] P. Skubic,[13] M. Wood,[13] M. Bishai,[14] J. Fast,[14] E. Gerndt,[14] J.W. Hinson,[14] D.H. Miller,[14] E.I. Shibata,[14] I.P.J. Shipsey,[14] M. Yurko,[14] M. Battle,[15] L. Gibbons,[15] S.D. Johnson,[15] Y. Kwon,[15] S. Roberts,[15] E.H. Thorndike,[15] C.P. Jessop,[16] K. Lingel,[16] H. Marsiske,[16] M.L. Perl,[16] S.F. Schaffner,[16] R. Wang,[16] T.E. Coan,[17] V. Fadeyev,[17] I. Korolkov,[17] Y. Maravin,[17] I. Narsky,[17] V. Shelkov,[17] R. Stroynowski,[17] J. Staeck,[17] I. Volobouev,[17] J. Ye,[17] M. Artuso,[18] A. Efimov,[18] M. Gao,[18] M. Goldberg,[18] R. Greene,[18] D. He,[18] S. Kopp,[18] G.C. Moneti,[18] R. Mountain,[18] Y. Mukhin,[18] T. Skwarnicki,[18] S. Stone,[18] X. Xing,[18] J. Bartelt,[19] S.E. Csorna,[19] V. Jain,[19] S. Marka,[19] A. Freyberger,[20] D. Gibaut,[20] K. Kinoshita,[20] I.C. Lai,[20] P. Pomianowski,[20] S. Schrenk,[20] G. Bonvicini,[21] D. Cinabro,[21] B. Barish,[22] M. Chadha,[22] S. Chan,[22] G. Eigen,[22] J.S. Miller,[22] C. O'Grady,[22] M. Schmidtler,[22] J. Urheim,[22] A.J. Weinstein,[22] F. Würthwein,[22] D.M. Asner,[23] M. Athanas,[23] D.W. Bliss,[23] W.S. Brower,[23] G. Masek,[23] H.P. Paar,[23] J. Gronberg,[24] C.M. Korte,[24] D.J. Lange,[24] R. Kutschke,[24] S. Menary,[24] R.J. Morrison,[24] S. Nakanishi,[24] H.N. Nelson,[24] T.K. Nelson,[24] C. Qiao,[24] J.D. Richman,[24] D. Roberts,[24] A. Ryd,[24] H. Tajima,[24] M.S. Witherell,[24] R. Balest,[25] B.H. Behrens,[25] K. Cho,[25] W.T. Ford,[25] M. Lohner,[25] H. Park,[25] P. Rankin,[25] J. Roy,[25] and J.G. Smith[25]

[1]Cornell University, Ithaca, New York 14853
[2]University of Florida, Gainesville, Florida 32611
[3]Harvard University, Cambridge, Massachusetts 02138
[4]University of Hawaii at Manoa, Honolulu, HI 96822
[5]University of Illinois, Champaign-Urbana, Illinois, 61801
[6]Carleton University, Ottawa, Ontario K1S 5B6 and the Institute of Particle Physics, Canada
[7]McGill University, Montréal, Québec H3A 2T8 and the Institute of Particle Physics, Canada

*Permanent address: BINP, RU-630090 Novosibirsk, Russia

[8]Ithaca College, Ithaca, New York 14850
[9]University of Kansas, Lawrence, Kansas 66045
[10]University of Minnesota, Minneapolis, Minnesota 55455
[11]State University of New York at Albany, Albany, New York 12222
[12]Ohio State University, Columbus, Ohio, 43210
[13]University of Oklahoma, Norman, Oklahoma 73019
[14]Purdue University, West Lafayette, Indiana 47907
[15]University of Rochester, Rochester, New York 14627
[16]Stanford Linear Accelerator Center, Stanford University, Stanford, California, 94309
[17]Southern Methodist University, Dallas, Texas 75275
[18]Syracuse University, Syracuse, New York 13244
[19]Vanderbilt University, Nashville, Tennessee 37235
[20]Virginia Polytechnic Institute and State University, Blacksburg, Virginia 24061
[21]Wayne State University, Detroit, Michigan 48202
[22]California Institute of Technology, Pasadena, California 91125
[23]University of California, San Diego, La Jolla, California 92093
[24]University of California, Santa Barbara, California 93106
[25]University of Colorado, Boulder, Colorado 80309-0390

CLEO [1] and ARGUS [2] have demonstrated a non-zero value for $|V_{ub}|$ by observing leptons from B-decays at the $\Upsilon(4S)$ with momenta greater than 2.4 GeV/c. This momentum range is accessible to $b \to u\ell\nu$ decays, but is rarely reached in the dominant $b \to c\ell\nu$ process. The values for $|V_{ub}/V_{cb}|$ of 5 to 10% obtained from these measurements have large theoretical uncertainties because the details of hadronization significantly affect the lepton spectrum near the endpoint.

Study of exclusive $b \to u\ell\nu$ channels provides an alternate route to $|V_{ub}|$. Here, the theoretical challenge is to calculate the form factors. For $B \to \pi\ell\nu$ and $B \to \rho\ell\nu$, this is an active field, encompassing relativistic and nonrelativistic quark models, lattice studies, QCD sum rules and dispersion relation studies. Experimentally, there is the CLEO upper limit [3] in the combined modes $\rho^-\ell^+\nu$, $\rho^0\ell^+\nu$, and $\omega\ell^+\nu$. This Letter presents a study of the decays $B^0 \to \pi^-\ell^+\nu$, $B^+ \to \pi^0\ell^+\nu$, $B^0 \to \rho^-\ell^+\nu$, $B^+ \to \rho^0\ell^+\nu$, $B^+ \to \omega\ell^+\nu$, and charge conjugate modes, where $\ell = e$ or μ. The study is based on an $\Upsilon(4S)$ data sample of 2.66 fb^{-1} (2.84×10^6 $B\bar{B}$ pairs) accumulated by the CLEO experiment at the Cornell Electron Storage Ring (CESR).

The CLEO detector [4] contains three concentric wire chambers that detect charged particles over 95% of the solid angle. A 1.5 T superconducting solenoid provides the magnetic field. The total momentum resolution is $\Delta p/p = 0.6\%$ for a 2 GeV/c particle. A CsI(Tl) electromagnetic calorimeter situated inside the solenoid detects electrons and photons over 98% of 4π. A reconstructed π^0 mass resolution of 6 MeV is typical.

The undetected neutrino complicates the analysis of semileptonic decays. Using the hermeticity of the CLEO detector, we reconstruct the neutrino by inferring its four–momentum from the missing energy ($E_{\rm miss} \equiv 2E_{\rm beam} - \sum E_i$) and the missing momentum ($\vec{P}_{\rm miss} \equiv -\sum \vec{p}_i$) in each event. In the process $e^+e^- \to \Upsilon(4S) \to B\bar{B}$, the total energy of the beams is imparted to the $B\bar{B}$ system. At CESR, the system is produced at rest, so the neutrino combined with the signal lepton and meson should satisfy the energy constraint $\Delta E \equiv (E_\nu + E_\ell + E_X) - E_{\rm beam} = 0$ and the momentum constraint $M_{\rm cand} \equiv [E^2_{\rm beam} - |\vec{p}_\nu + \vec{p}_\ell + \vec{p}_X|^2]^{\frac{1}{2}} = M_B$, where X is the final state meson.

To suppress events in which $\vec{P}_{\rm miss}$ misrepresents $\vec{p}_\nu$, we reject those with multiple leptons or a non-zero total charge because they indicate other missing particles. We further require that $M^2_{\rm miss} \equiv E^2_{\rm miss} - |\vec{P}_{\rm miss}|^2$ be consistent with zero. Surviving signal events show a resolution in $|\vec{p}_{\rm miss}|$ of about 110 MeV/c. Because the resolution on $E_{\rm miss}$ is about 2.5 times larger, we take $(E_\nu, \vec{p}_\nu) = (|\vec{p}_{\rm miss}|, \vec{p}_{\rm miss})$.

Information from specific ionization and from the calorimeter and tracking measurements is combined to identify electrons with $p > 600$ MeV/c over 90% of the solid angle. Particles registering hits in muon counters at least 5 interaction lengths deep over the polar angle range $|\cos\theta| < 0.85$ are considered muons. Counters at 3 interaction lengths within $|\cos\theta| < 0.71$ are used for the multiple-lepton veto. Candidate leptons must have $p_\ell > 1.5$ GeV/c for the π modes and $p_\ell > 2.0$ GeV/c for the ρ and ω (vector) modes. The π modes have a softer p_ℓ spectrum since transverse W helicities are forbidden in those decays. The identification efficiency above 1.5 GeV/c is typically over 90%; the probability that a hadron is misidentified as a signal electron (muon), a "fake lepton", is approximately 0.1% (1%).

A π^0 candidate must have a $\gamma\gamma$ invariant mass within 2 standard deviations of the π^0 mass. We study the ω via its $\pi^+\pi^-\pi^0$ decay, suppressing combinatoric background by rejecting combinations away from the center of the ω Dalitz plot. Discrimination of the

broad ρ resonances from nonresonant $\pi\pi\ell\nu$ decay is discussed below.

There are backgrounds from $e^+e^- \to q\bar{q}, \tau^+\tau^-$ continuum events, fake leptons, $b \to c\ell\nu$ decays, and other $b \to u\ell\nu$ decays. Eliminating jet-like events (event axes based on signal particles and on all other particles are roughly parallel) suppresses continuum backgrounds 10-fold and retains 70% of the signal. We subtract the residual continuum background using data accumulated at an energy 60 MeV below the $\Upsilon(4S)$ energy. We determine the background from fake leptons by applying measured fake rates to nonleptonic data. The lepton momentum requirement eliminates background from $b \to c \to s\ell\nu$ and reduces the $b \to c\ell\nu$ contamination. Monte Carlo (MC) studies indicate that most $b \to c\ell\nu$ events in the final sample either contain a K_L or have $c \to s\ell\nu$ with the lepton not identified.

We fit the π (ρ) data in two (three) dimensions to extract the rate. For all modes the data are divided into 11 bins over the $(M_{\rm cand}, \Delta E)$ region $5.1075 \leq M_{\rm cand} < 5.2875$ GeV and $|\Delta E| < 0.75$ GeV. A signal bin is defined by $5.265 \leq M_{\rm cand} < 5.2875$ GeV, $-0.15 \leq \Delta E < 0.25$ GeV. The neutrino dominates the resolution in $M_{\rm cand}$ (± 7 MeV) and ΔE (± 110 MeV). To help distinguish resonant from nonresonant final states in the $\rho\ell\nu$ ($\omega\ell\nu$) modes, we further divide the yields into five (four) equal bins over the $\pi\pi$ (3π) mass range within ± 475 MeV (-60 MeV to $+100$ MeV) of the nominal ρ (ω) mass.

MC simulation provides the shapes in $M_{\rm cand}$, ΔE and $\pi\pi$ or 3π mass for the five signal modes, the $b \to c$ background in each mode, the crossfeed among the modes, and the feeddown from higher mass $B \to X_u\ell\nu$ decays. The simulation includes a full description of the $b \to c$ and charm decay modes and a GEANT-based [5] detector model. Feeddown from other $X_u\ell\nu$ decays was evaluated with the ISGW II model [6] for all resonances through the $\rho(1450)$. We fixed the rate for these decays from the observed rate near the lepton-momentum endpoint [1]. To estimate model dependence, the efficiencies and the signal and crossfeed shapes are completely redetermined for several models.

We fit the continuum- and fake-subtracted distributions in the five modes simultaneously. The isospin and quark symmetry relations $\Gamma(B^0 \to \pi^-\ell^+\nu) = 2\Gamma(B^+ \to \pi^0\ell^+\nu)$ and $\Gamma(B^0 \to \rho^-\ell^+\nu) = 2\Gamma(B^+ \to \rho^0\ell^+\nu) \approx 2\Gamma(B^+ \to \omega\ell^+\nu)$ constrain the B^+ rates relative to the B^0 rates. Hence we fit for two independent efficiency-corrected yields, $N_{\pi^\pm}$ and $N_{\rho^\pm}$. For self-consistency, the crossfeed rates are constrained by the observed yields. The $b \to c$ background normalization in the fit varies independently for each mode. The normalizations obtained are consistent with that derived from the luminosity and the $\Upsilon(4S)$ production cross section. A typical χ^2 is 145 for 169 degrees of freedom.

We have evaluated a variety of models: ISGW II (a nonrelativistic quark model) [6]; relativistic quark model calculations [7–9]; and a hybrid model that uses a dispersion-relation-based calculation of the $\pi\ell\nu$ form factor [10], and combines lattice calculations of the $\rho\ell\nu$ form factors [11] with predicted $\rho\ell\nu$ form factor relations [12,13]. Model dependence results because the lepton-momentum requirements cause the reconstruction efficiencies to vary with q^2. Further dependence of efficiencies on q^2 have been minimized. There is also model dependence in the fitted signal yields (before efficiency correction) because the reconstruction and crossfeed probabilities have different q^2 dependences.

In Fig. 1 we show the $M_{\rm cand}$ distribution for data in the ΔE signal band for the combined π modes and the combined vector modes. An excess over background is apparent in both. The lepton momentum spectra for events in the $(M_{\rm cand}, \Delta E)$ signal bin are also plotted in Fig. 1. Significant rates beyond the $b \to c\ell\nu$ endpoint are clear. Table I lists the data

TABLE I. Summary of data yields in the signal bin and the corresponding ISGW II [6] efficiencies and fit results. The errors on the fitted signal yields within the two π modes (three vector modes) are completely correlated.

	$\pi^{\pm}$	π^0	$\rho^{\pm}$	ρ^0	ω
$\Upsilon(4S)$ yield	46	19	47	73	7
Continuum+fake bkg.	9.8 ± 2.1	1.5 ± 0.5	9.5 ± 2.1	5.8 ± 1.2	0.3 ± 0.8
Efficiency (ISGW II)	0.023	0.015	0.015	0.024	0.006
fit signal yield	26.6 ± 6.1	8.6 ± 2.0	19.5 ± 3.3	15.1 ± 2.5	3.5 ± 0.6
$b \to c$ bkg.	7.0 ± 1.2	2.9 ± 0.8	15.2 ± 1.8	21.5 ± 2.2	4.6 ± 1.1
$b \to u$ bkg.	0.5 ± 0.1	0.2 ± 0.1	2.7 ± 0.2	2.9 ± 0.2	0.5 ± 0.1
crossfeed bkg.	4.1 ± 0.8	1.5 ± 0.3	4.9 ± 0.9	13.4 ± 2.5	0.8 ± 0.2

yields and the continuum and fake lepton backgrounds in the signal bin, as well as the corresponding fit yields from the ISGW II fit. The 2π (3π) mass interval ± 270 MeV (± 20 MeV), where the ρ (ω) candidates are expected, is used for yields and figures. The $\pi\pi$ and 3π mass distributions for the combined $\rho\ell\nu$ modes and for the $\omega\ell\nu$ mode are shown in Fig. 2. A clear excess is observed near the ρ mass. The $\omega\ell\nu$ mode is consistent both with pure background and with the signal level expected given the $\rho\ell\nu$ rate.

To check for nonresonant $\pi\pi\ell\nu$ contributions, we have compared the fit just described to fits restricting the $\pi\pi$ (3π) mass distribution in the $\rho\ell\nu$ ($\omega\ell\nu$) modes to a single bin of width 90 (20) MeV, with and without subtracting the ΔE vs. $M_{\rm cand}$ distribution in $\pi\pi$ (3π) mass sidebands from the mass peak distribution. These fits give results consistent with those obtained above, suggesting that any nonresonant contribution is small. We have also studied $B \to \pi^0\pi^0\ell\nu$, which can have only nonresonant signal contributions, and have found that our predicted crossfeed from the ρ modes is consistent with saturating the observed rate. We limit the bias in the $\rho\ell\nu$ ($\pi\ell\nu$) branching fraction from nonresonant contamination to 20% (5%) by studying fits that include the $B \to \pi^0\pi^0\ell\nu$ mode and a nonresonant component generated from an inclusive spectator $b \to u\ell\nu$ model and a $\pi\pi$ mass spectrum that is either a ρ line-shape or the dipion-mass shape from a hadronization model.

Table II summarizes the contributions to the systematic errors. Uncertainty in the assumed decay of the second B in the event and inaccuracies in detector simulation constitute the dominant systematic error. These effects were investigated by varying the K_L^0 fraction, charm semileptonic decay rate, charged particle and photon-finding efficiencies, false charged particle and false photon rejection efficiencies, charged particle momentum resolution, and photon energy resolution. Changes due to variations in the mix of the $B \to D^{(*)}X\ell\nu$ rates used in the $B\bar{B}$ MC are small, as are changes from variation of the rate of feeddown from higher mass $B \to X_u\ell\nu$.

The branching fractions for $B^0 \to \pi^-\ell^+\nu$ and $B^0 \to \rho^-\ell^+\nu$ are given in Table III for each model. The model predictions of the ρ/π ratio are generally consistent with our data. However, the probability that the KS model is consistent with our observed ratio is less than 0.5%, so we have chosen to exclude this model from any averaging. From the remaining models considered we obtain $\mathcal{B}(B^0 \to \pi^+\ell^-\nu) = (1.8 \pm 0.4 \pm 0.3 \pm 0.2) \times 10^{-4}$ and $\mathcal{B}(B^0 \to \rho^+\ell^-\nu) = (2.5 \pm 0.4^{+0.5}_{-0.7} \pm 0.5) \times 10^{-4}$, where the first error is statistical, the second is systematic, and the third is an estimate of the model uncertainty based on the spread of

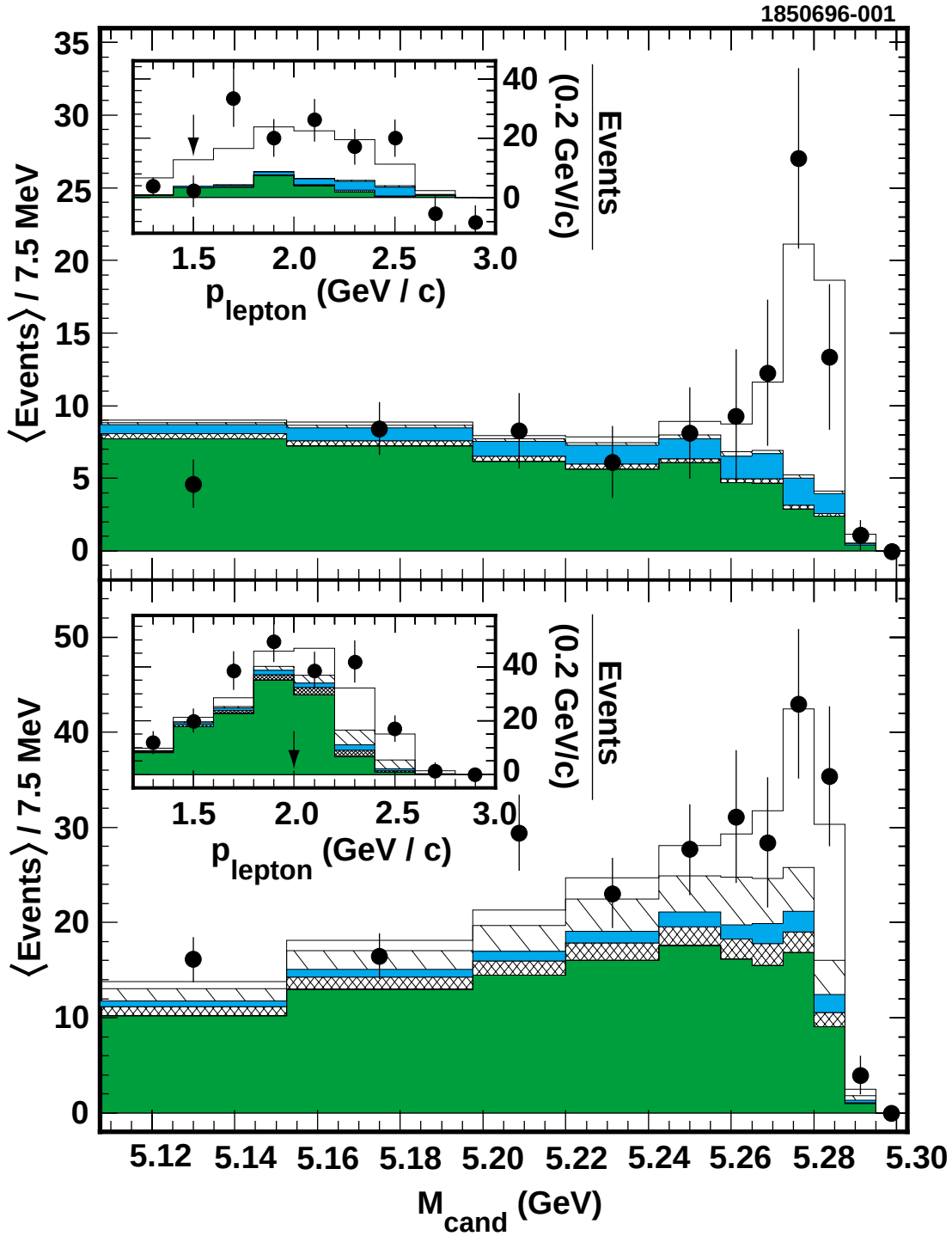

FIG. 1. The $M_{\rm cand}$ mass distributions in the ΔE signal band and the signal-bin lepton-momentum spectra (insets) for the combined π modes (top) and the combined vector modes (bottom). The points are the data after continuum and fake background subtractions; the dark shaded, cross-hatched and unshaded histograms are $b \to cX$, $b \to u\ell\nu$ feeddown, and signal respectively. For the π (vector) modes, the light-shaded and hatched histograms are $\pi \to \pi$ (vector $\to$ vector) and vector $\to \pi$ ($\pi \to$ vector) crossfeed, respectively. The histogram normalizations are from the nominal fit. The arrows indicate the momentum cuts.

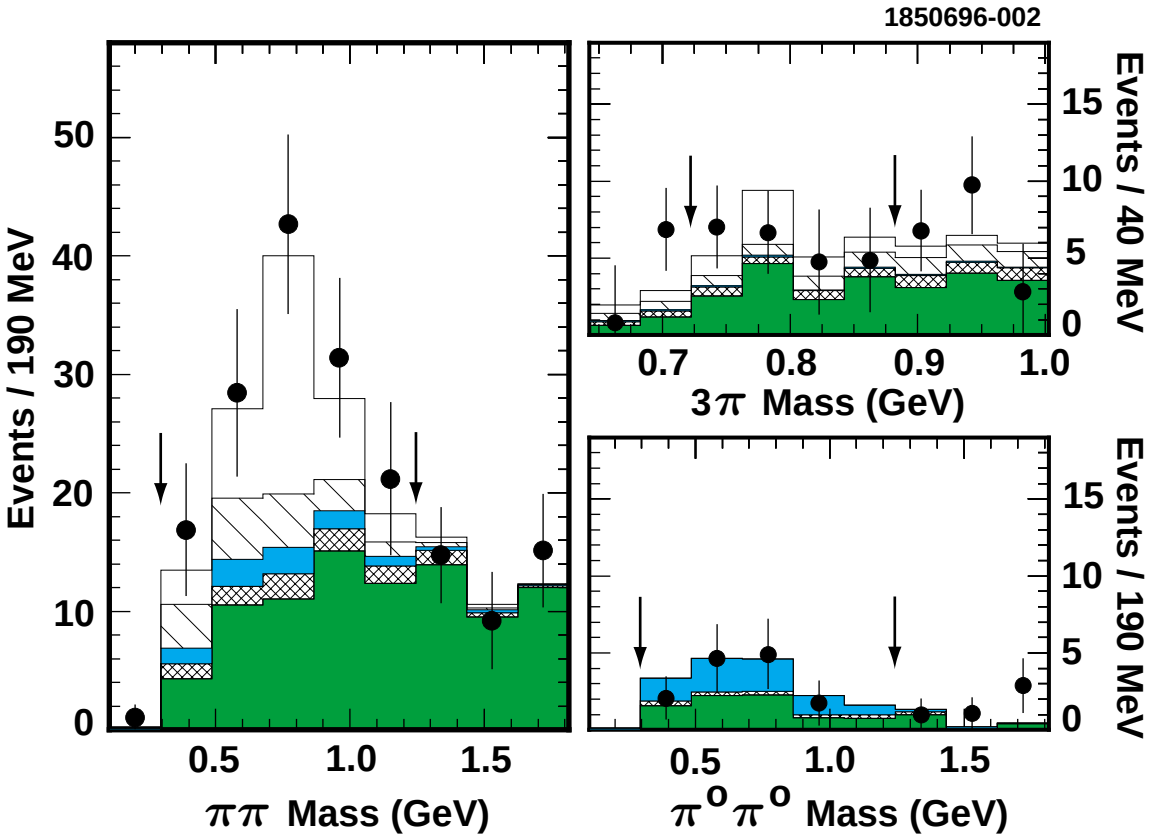

FIG. 2. Reconstructed mass distributions for $\rho \to \pi\pi$ (left), $\omega \to 3\pi$ (top right) and for $\pi^0\pi^0$ from $B \to \pi^0\pi^0\ell\nu$ (bottom right) in the $(M_{\rm cand}, \Delta E)$ signal bin. Fig. 1 describes the histogram shadings and normalization. The arrows indicate the mass range considered when fitting.

TABLE II. Contributions to the systematic error (%) in each branching fraction ($\mathcal{B}$) and the ratio of rates. Simulation of the detector and the second B contribute to ν simulation.

Source	$\mathcal{B}_\pi$	$\mathcal{B}_\rho$	ratio
ν simulation	14.5	14.8	12.7
$B \to D/D^* X\ell\nu$	2.1	3.2	3.9
fakes+continuum	5.4	6.7	8.6
$b \to u\ell\nu$ feeddown	2.2	7.5	9.8
lepton ID	2.0	2.0	2.0
luminosity	2.0	2.0	–
$f_{+-}\tau_+/f_{00}\tau_0$	3.2	1.9	3.3
nonresonant $\pi\pi\ell\nu$	-5.0	-20.0	-16.0
Total	+16.3	+18.4	+19.0
	-17.0	-27.2	-24.8

models and individual model errors. The average ρ/π rate ratio is $1.4^{+0.6}_{-0.4}\pm0.3\pm0.4$. For each model, the branching fractions, the isospin relations and the predicted p_ℓ spectral shapes for the five modes can be combined to obtain a total rate into the $2.4 < p_\ell < 2.6$ GeV/c (where π, ρ and ω should be the dominant $X_u\ell\nu$ modes) and the $2.3 < p_\ell < 2.6$ GeV/c (used for the inclusive $|V_{ub}|$ measurements) intervals. We find our rate in the smaller endpoint region to be consistent with saturating the rate from the most recent CLEO endpoint study [1], and we obtain a 90% C.L. upper limit of 0.44×10^{-4} for the contribution of all other modes. For the broader range, we obtain the limit 1.03×10^{-4}.

We extract values for $|V_{ub}|$ from these branching fractions using the predicted partial widths. We take $\tau_{B^0} = 1.56 \pm 0.05$ ps and $\tau_{B^0}/\tau_{B^+} = 1.02 \pm 0.04$ [14]. Table III lists the results. To obtain $|V_{ub}|_{\rm avg}$, the π and ρ modes were combined by fixing their ratio to the prediction for each model. Correlations in the modes from our fitting procedure are thereby automatically accounted for; we also account for correlated systematics. Averaging over the values of $|V_{ub}|$ obtained from these models, we have $|V_{ub}| = (3.3 \pm 0.2^{+0.3}_{-0.4} \pm 0.7) \times 10^{-3}$, where the errors are statistical, systematic (including the B^0 lifetime) and estimated model dependence. This agrees with the value of $|V_{ub}|$ obtained from the inclusive endpoint rate [1].

These are the first exclusive $b \to u$ branching fractions measurements. The agreement between the $|V_{ub}|$ obtained here and from the inclusive analysis lends considerable confidence to our knowledge of $|V_{ub}|$.

We thank G. Burdman, J. Flynn, N. Isgur, D. Scora and B. Stech for advice on and assistance with form factor models. We gratefully acknowledge the effort of the CESR staff in providing us with excellent luminosity and running conditions. This work was supported by the National Science Foundation, the U.S. Department of Energy, the Heisenberg Foundation, the Alexander von Humboldt Stiftung, the Natural Sciences and Engineering Research Council of Canada, and the A.P. Sloan Foundation.

TABLE III. Final results for each model considered. We define $\Gamma_X \equiv \gamma_X |V_{ub}|^2 \equiv 10^{12} \times \Gamma(B^0 \to X^- \ell^+ \nu)$ and $\mathcal{B}_X \equiv \mathcal{B}(B^0 \to X^- \ell^+ \nu)$. $\Delta\chi^2$ is the χ^2 change from the preferred fit to a fit with γ_ρ/γ_π fixed to the prediction (systematics included). The statistical errors on the ratio are defined by $\Delta\chi^2 = 1$; as the asymmetric errors and the χ^2 changes indicate, these errors are highly nongaussian. Third errors, where given, arise from the model's estimated form-factor uncertainties.

Model	ISGW II [6]	WSB [7]	KS [8]	Melikhov [9]	Hybrid [10–13]
γ_ρ,γ_π (s^{-1})	14.2, 9.6	26.1, 7.4	33.0, 7.3	11.8 ± 3.4, 7.6 ± 1.7	13.8 ± 4.0, 13.5 ± 9.1
$\mathcal{B}_\pi/10^{-4}$	$2.0 \pm 0.5 \pm 0.3$	$1.8 \pm 0.5 \pm 0.3$	$1.9 \pm 0.5 \pm 0.3$	$1.8 \pm 0.4 \pm 0.3 \pm 0.2$	$1.7 \pm 0.4 \pm 0.3 \pm 0.2$
$\mathcal{B}_\rho/10^{-4}$	$2.2 \pm 0.4^{+0.4}_{-0.6}$	$2.8 \pm 0.5^{+0.5}_{-0.8}$	$1.9 \pm 0.3^{+0.4}_{-0.5}$	$2.8 \pm 0.5^{+0.5}_{-0.8} \pm 0.4$	$2.1 \pm 0.4^{+0.4}_{-0.6} \pm 0.4$
Γ_ρ/Γ_π	$1.1^{+0.5+0.2}_{-0.3-0.3}$	$1.6^{+0.7+0.3}_{-0.5-0.4}$	$1.0^{+0.5+0.2}_{-0.3-0.3}$	$1.6^{+0.7+0.3}_{-0.5-0.4} \pm 0.11$	$1.2^{+0.6+0.2+0.2}_{-0.4-0.3-0.1}$
$\Delta\chi^2$	0.5	3.1	8.1	0.2	0.4
$\lvert V_{ub}\rvert_\pi$	$3.7 \pm 0.4 \pm 0.3$	$4.0 \pm 0.5 \pm 0.3$	$4.1 \pm 0.5 \pm 0.3$	$3.9 \pm 0.5 \pm 0.3 \pm 0.5$	$2.9 \pm 0.3 \pm 0.2^{+1.3}_{-0.7}$
$\lvert V_{ub}\rvert_\rho$	$3.2 \pm 0.3^{+0.3}_{-0.4}$	$2.6 \pm 0.2^{+0.2}_{-0.4}$	$2.0 \pm 0.2^{+0.2}_{-0.3}$	$4.0 \pm 0.4^{+0.4}_{-0.5} \pm 0.6$	$3.1 \pm 0.3^{+0.3+0.3}_{-0.4-0.4}$
$\lvert V_{ub}\rvert_{\rm avg}$	$3.4 \pm 0.2^{+0.3}_{-0.4}$	$2.9 \pm 0.2^{+0.3}_{-0.3}$	$2.2 \pm 0.1^{+0.2}_{-0.3}$	$4.0 \pm 0.2^{+0.35}_{-0.5} \pm 0.5$	$3.1 \pm 0.2^{+0.3}_{-0.4} \pm 0.5$

REFERENCES

[1] R. Fulton *et al.*, Phys. Rev. Lett. **64**, 16 (1990); J. Bartelt *et al.*, Phys. Rev. Lett. **71**, 4111 (1993).

[2] H. Albrecht *et al.*, Phys. Lett. B **234**, 409 (1990); and Phys. Lett. B **255**, 297 (1991).

[3] A. Bean *et al.*, Phys. Rev. Lett. **70**, 2681 (1993).

[4] Y. Kubota *et al.*, Nucl. Instrum. Methods Phys. Res., Sect. A **320**, 66 (1992).

[5] R. Brun *et al.*, GEANT 3.15, CERN DD/EE/84-1.

[6] N. Isgur and D. Scora, Phys. Rev. D **52**, 2783 (1995). See also N. Isgur *et al.*, Phys. Rev. D **39**, 799 (1989). The authors state errors on the predicted rates of 25% to 50%.

[7] M. Wirbel, B. Stech and M. Bauer, Z. Phys. C **29**, 637 (1985).

[8] J.G. Körner and G.A. Schuler, Z. Phys. C **38**, 511 (1988).

[9] D. Melikhov, Phys. Rev. D **53**, 2160 (1996); Preprint hep-ph/9603340.

[10] G. Burdman and J. Kambor, FNAL preprint FERMILAB-Pub-96/033-T, Feb., 1996. We take $F_B = 180 \pm 40$ MeV and $g = 0.5 \pm 0.2$.

[11] J.M. Flynn *et al.*, Nucl. Phys. B **461**, 327 (1996); J.M. Flynn *et al.*, Grenada preprint UG-DFM-3-96, Feb. 1996.

[12] B. Stech, Phys. Lett. B **354**, 447 (1995); B. Stech, to appear in *Proceedings of the Strasbourg Conference*, Sept. 1995.

[13] We fit UKQCD lattice form factor calculations [11] using the relations $A_0(t)/(1+\zeta_{A_0}(t)) = V(t)/(1+\zeta_V(T)) = f_{0V}/(1-t/m_{0V})^n$ and $A_2(t)/(1+\zeta_{A_2}(t)) = A_1(t)/[(1-t/(m_B^2+m_\rho^2)^2)(1+\zeta_V(T))] = f_{12}/(1-t/m_{12})^n$, and the constraint $2m_\rho A_0(0) = (m_B+m_\rho)A_1(0) - (m_B-m_\rho)A_2(0)$. The $\zeta(t)$ functions are taken from [12]. For $n=2$, we find $m_{12} = 5.94 \pm 0.17$ GeV, $m_{0V} = 5.42 \pm 0.13$ GeV, and $f_{V0} = 0.36 \pm 0.04$. These parameters and n are varied to explore the uncertainties from the lattice results and our functional form.

[14] I.J. Kroll, FNAL preprint FERMILAB-CONF-96-032, Feb., 1996. To appear in *Proceedings of the XVII International Symposium on Lepton-Photon Interactions*, Beijing, 10-15 August 1995.